Yeager and Advani *Integrating Materials and Manufacturing Innovation* (2015) 4:3
DOI 10.1186/s40192-015-0032-1

Integrating Materials and Manufacturing Innovation
a SpringerOpen Journal

RESEARCH ARTICLE Open Access

Numerical model of fiber wetting with finite resin volume

Michael Yeager and Suresh G Advani*

* Correspondence: advani@udel.edu
Department of Mechanical Engineering and Center for Composite Materials, University of Delaware, Newark, DE 19716, USA

Abstract

The partial wetting of cylindrical surfaces is encountered in many industrial applications such as composites manufacturing, MEMS, hair care products, and textile engineering. Understanding the impact of key parameters such as resin and fiber surface interaction properties and the geometric arrangement of the fibers on wetting would lead to tailoring a desired interface between the resin and the fiber surface. A three-dimensional model of resin wetting a single fiber is presented. This model is then extended to study a finite volume of resin wetting fibers in square and triangular packing arrangements. The impact of changing wetting properties and fiber volume fraction is examined for each packing arrangement.

Keywords: Wetting; Contact angle; Computational multiphase flow; Composites

Background

The partial wetting of cylindrical surfaces by a finite volume of resin is an important phenomenon in many industrial applications such as composites manufacturing, MEMS, and textile engineering. A constitutive equation governing the partial wetting of a finite volume of liquid on a flat plate has been formulated and reported [1]. The equilibrium shape of resin on single fibers has also been studied in depth [2-5]. Carroll [2] was the first to develop an analytical solution for the equilibrium shape of a resin drop on a single fiber. A drop at rest on a fiber will either conform to a "barrel" geometry, where the drop wraps around the fiber, or a "clamshell" geometry in which the fiber rests on the fiber's surface without wrapping around it. A phase diagram predicting which of these configurations a particular drop will adopt has been constructed [5].

An analytical solution for the equilibrium shape of a liquid drop on a fiber surface was first derived by Carroll [2]. Wu and Dzenis later developed an analytical solution to this problem using an energy approach [4]. Both of these solutions assume an axisymmetric shape. The equations necessary to determine the maximum height of the drop on the fiber and the length of contact between the fiber and resin are given in [2,4] and reproduced below:

$$y^2 = {y_0}^2\left(1-k^2 sin^2\phi\right) \tag{1}$$

$$x = \pm[\lambda r F(k,\phi) + y_0 E(k,\phi)] \tag{2}$$

Here, x is the location on the axis of the fiber measured from the center of the drop, and y is the height of the drop, measured from the axis of the fiber. y_0 is the maximum

height of the drop measured from the axis of the fiber, and r is the fiber radius. $E(k,\phi)$ and $F(k,\phi)$ are Legendre's elliptical functions of the second and first kind, respectively. Here λ and k are defined as follows:

$$\lambda = \frac{y_0 \cos\theta - r}{y_0 - r\cos\theta} \tag{3}$$

$$k^2 = 1 - \lambda^2 \left(\frac{r}{y_0}\right)^2 \tag{4}$$

Here, θ is the static contact angle between the fiber and resin.

The final wetted length, L, which is also defined in Figure 1, can be calculated using the known volume V once y_0 is solved for with the above equations and:

$$L = 2[\lambda r F(k, \phi_0) + y_0 E(k, \phi_0)] \tag{5}$$

$$V = 2\pi \int_r^{y_0} \frac{y^2(y^2 + \lambda r y_0)}{\sqrt{(y_0{}^2 - y^2)(y^2 - \lambda^2 r^2)}} dy - \pi r^2 L \tag{6}$$

ϕ_0 is found through setting $y = 0$ in Equation 1.

There have also been other investigations with resin spreading within multiple fibers, for example final resin configuration between two parallel fibers has been studied with relation to static contact angle, filament spacing, resin volume, and fiber diameter [6]. The axial wetting of a single fiber from a reservoir of resin has been experimentally examined and constitutive equations have been developed to describe this phenomenon [7]. The dynamics of a finite volume of resin spreading on a single fiber has yet to be explored and is the subject of this paper. Trends seen with the dynamics of resin wetting a single fiber hold true for systems with multiple fibers.

A numerical model is presented using the level set method to study the movement and spreading of a finite volume of resin on any planar or curvilinear surface. The method and accuracy is verified by comparing the model results with experiments conducted of a drop spreading on a flat plate. The method is then used to describe the wetting dynamics of a finite drop of resin on a single fiber. The model is further extended to investigate the flow of finite volume resin within multifiber unit cells representing square and hexagonal fiber packing arrangements, which are commonly used

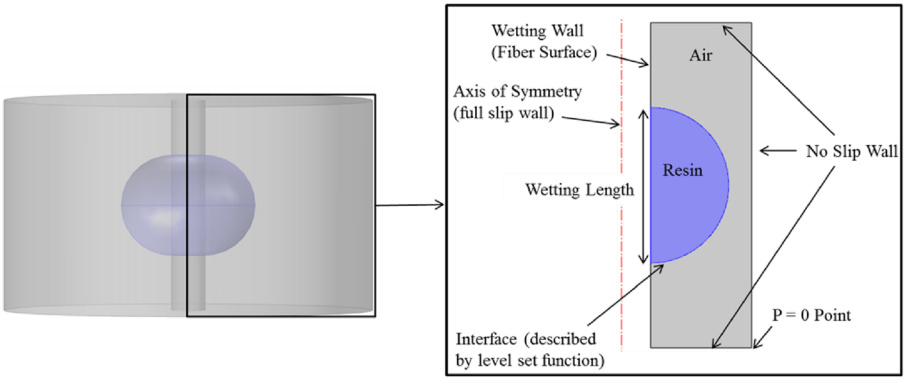

Figure 1 Axisymmetric single-fiber model.

in composites. The use of a finite volume of resin is necessary because there are situations where it is desirable to strategically create microvoids to increase the composite's energy-absorption capabilities. Each tow would be a porous structure comprised of a series of microstructures represented by the unit cells. The model studies the impact of key composite-processing properties on the fiber-matrix interfacial area. Through examination of the interfacial area instead of the contact length, one is better able to understand the impact of manipulating processing parameters on the resulting composite properties. This investigation should prove useful in tailoring the interface properties between fibers and resin as a function of the resin and fiber surface properties and the fiber arrangement.

Methods

Model setup

The numerical models were developed using the COMSOL Multiphysics and the Microfluidics Module to investigate the dynamics of wetting over a single fiber and within unit cells of multiple fibers with a finite volume of resin and are presented below. A model was also constructed of a drop spreading on a flat plate with the goal of experimentally validating the solution method.

Axisymmetric single-fiber model

Figure 1 shows the axisymmetric single-fiber model. In this model, a spherical drop of resin is initially enveloping the fiber. This simplifies the resin movement to be along the fiber surface in the axial direction. An axis of symmetry is utilized to increase computational efficiency. The axis of symmetry is the center of the fiber with a full-slip condition (symmetry condition), which sets the derivative of the tangential velocity equal to zero along the axis. The no-slip boundary condition is applied along the walls shown in Figure 1 where the velocity is set to zero. The pressure is set equal to zero, the reference pressure, at a single point to ensure that the pressure solution is unique [8]. This is needed because the Navier–Stokes equations only solve for the gradient of pressure. The wetting wall is the surface of the fiber along which the resin moves and employs a slip length and the final static contact angle to drive the wetting and spread the resin, both of which will be discussed in a later section. The fiber diameter was 9 μm. These baseline values, shown in Table 1, were selected based on resin and fiber systems used in composites processing.

Three-dimensional single-fiber model

The three-dimensional representation of a drop of resin spreading on a single fiber is depicted in Figure 2. The resin drop diameter to fiber radius ratio in this model is

Table 1 Baseline properties used for parametric studies for the axisymmetric single-fiber model as well as the three- and four-fiber unit cells

Baseline properties used for axisymmetric single-fiber model and fiber unit cells	
Resin density	1.17 g/cm^3
Resin viscosity	9.5 Pa·s
Static contact angle	30°
Resin surface tension	0.07 J/m^2
Slip length (β)	0.1 μm

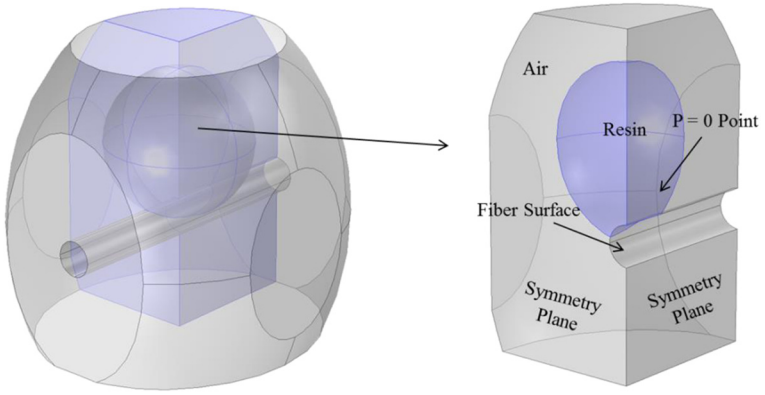

Figure 2 Three-dimensional single-fiber model.

intentionally large. This is because we desire the equilibrium position of the resin to be in the "barrel" shape. A fiber radius of 3 μm, resin volume of 2,280 μm^3, and contact angle of 15° were selected to ensure that the final shape is a "barrel" guided by the studies performed by Eral et al. [5]. The other important properties are the same as the baseline values described in Table 1.

Unit cell with square and triangular packing arrangements

The square and triangular fiber packing-arrangement unit cells are shown in Figure 3. Flow in each unit cell is simplified through the use of symmetry planes to increase computational efficiency. The four-fiber unit cell has three planes of symmetry due to the assumption that gravity is negligible, which will be discussed later. The fiber surfaces are wetting walls, and walls other than fiber surfaces and symmetry planes are no-slip walls. Both models also include a point where the pressure is set equal to zero. The pressure is set equal to zero at a reference location, to ensure that the pressure solution is unique. The fiber radius was 4 μm. The baseline values for the resin and interaction parameters can be found in Table 1.

Resin spreading on a flat plate

A numerical model of the drop of glycerin, shown in Figure 4, was developed to compare the numerical solution and experimental results. The glycerin properties were found using traditional characterization techniques, described and reported in the "Experimental setup

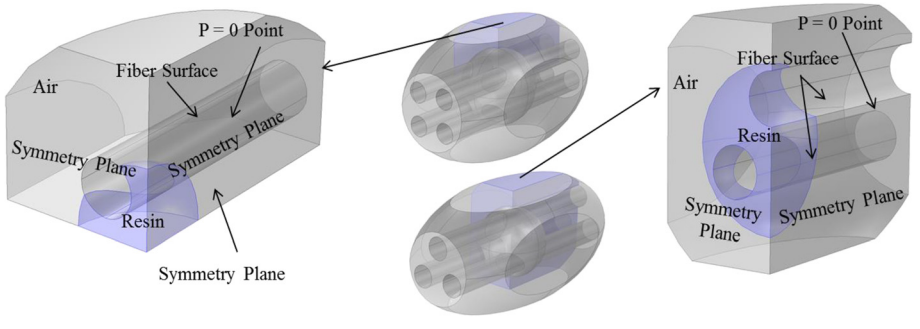

Figure 3 Schematic of three- and four-fiber unit cell models.

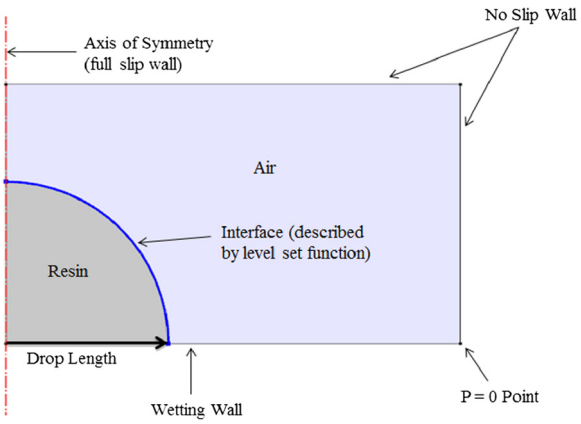

Figure 4 Schematic of single-drop spreading model.

and procedure" section. The properties for the air phase were taken from the COMSOL material library. The two-dimensional model takes advantage of the axisymmetric property of the process being modeled.

Assumptions

The Reynolds number in this problem is on the order of 10^{-8}; thus, it can be assumed that the inertial forces are negligible relative to the viscous forces and the Navier–Stokes equations can be reduced to the Stokes flow equations. The ratio of gravitational to capillary forces, represented by the bond number, is on the order of 10^{-6}, making it acceptable to neglect gravity. For the axisymmetric model, due to the geometry being symmetric about the fiber axis and our assumption of no gravity, the flow is considered axisymmetric about the axis of the fiber. It is assumed that the resin used does not cure during the wetting process, allowing us to maintain a constant viscosity value during the flow. It is also assumed that the fibers are rigid and do not move as the resin flows.

Governing equations

The governing equations (Equations 7 and 8) in the model are the Stokes and continuity equations. The interface between the two fluids is tracked using the level set method [9]. The level set method creates an interface with a finite thickness, described by the level set variable (ϕ), which continuously changes from 0 to 1 across the interface using a smeared out Heaviside function [10]. These equations (Equation 9), modified to account for the stated assumptions, are given by [11]:

$$\rho \cdot \boldsymbol{u}_t = -\nabla \cdot \boldsymbol{p} + \mu \nabla^2 \boldsymbol{u} + \boldsymbol{F}_{st} \tag{7}$$

$$\nabla \cdot \boldsymbol{u} = 0 \tag{8}$$

$$\phi_t + \boldsymbol{u} \cdot \nabla \phi = \sigma \nabla \cdot \left(\varepsilon \nabla \phi - \phi(1-\phi) \frac{\nabla \phi}{|\nabla \phi|} \right) \tag{9}$$

Where $\boldsymbol{u}$ is the velocity vector, the subscript denotes the partial derivative with respect to that variable, μ is the viscosity, $\boldsymbol{p}$ is the pressure, $\boldsymbol{F}_{st}$ is the force due to surface tension, σ is the reinitialization parameter for the interface, ε is the interface thickness, and ϕ is the level set variable. To minimize computational cost, the interface thickness

is set to one half of the largest element length [11,12]. The interfacial tension term is implemented using the continuous surface force formulation, given by:

$$F_{st} = \nabla \cdot \left(\gamma\left(\boldsymbol{I} - \boldsymbol{nn}^{\boldsymbol{T}}\right)\right)\boldsymbol{\delta} \tag{10}$$

$$\delta = 6|\nabla\phi||\phi(1-\phi)| \tag{11}$$

Here, γ is the surface tension of the resin-air interface, and δ is a Dirac delta function.

The density and viscosity within the interface between the resin and air are found using rule of mixtures [11]:

$$\rho = \rho_{\text{Resin}} + \left(\rho_{\text{Air}} - \rho_{\text{Resin}}\right)\phi \tag{12}$$

$$\mu = \mu_{\text{Resin}} + \left(\mu_{\text{Air}} - \mu_{\text{Resin}}\right)\phi \tag{13}$$

Fiber and resin parameters

The properties of the resin and the fiber-resin interactions play an important role in the wetting of the fibers by the resin. The viscosity of the resin has a large impact on the rate of wetting, but not a significant effect on the final shape of the drop. The bond number is the ratio of surface forces to body forces, providing a good indication if the resin flow is driven by surface forces or gravity. This study focuses on flows with low-bond numbers. The contact angle between the fiber and resin, largely impacted by the surface tension of the resin, represents the principle force driving wetting at the microscale. The fiber diameter and resin droplet size will be important geometrical parameters when investigating drops spreading on the fiber surfaces. When the model is extended to include multiple fibers, the fiber spacing and packing arrangement will influence the wetting dynamics.

Static contact angle between fiber and resin

Wetting describes the spreading of a liquid on a solid substrate [13]. The wettability of a substrate by a liquid wetting rate and region is quantified by the static contact angle, a force balance at the line of contact between the fiber surface (solid (s)), resin (liquid (l)), and air (vapor (v)) and is given by Young's equation [13]:

$$\cos\theta = \frac{\gamma_{sv} - \gamma_{sl}}{\gamma_{lv}} \tag{14}$$

In Young's equation, γ_{ij} represents the surface energy at the i-j interface. As shown in Equation 14, the final static contact angle takes into account both the resin surface tension and the difference in interfacial energies of the solid-vapor and solid–liquid interfaces. The solid-vapor and solid–liquid surface energies can be manipulated by modifying the fiber sizing, which is a coating that is applied to the fiber surface. The final static contact angle of the resin on the fiber surface has been shown to have a direct relationship with the interfacial shear strength of the resulting composite [14].

Resin viscosity

The viscosity of the resin does not affect the final position of the resin on the fibers since it is assumed to be constant. As the Stokes solution is linear, the time it takes to wet the fiber surface will be directly proportional to the viscosity of the resin.

Slip length

There are stress and velocity singularities at the three-phase contact line when solving the Stokes equations with a no-slip condition at the solid surface [15]. A way to handle this boundary condition is to move the "no-slip" condition to a plane located a distance β (slip length) below the solid surface and assume simple shear flow in the region between the wall and the no-slip plane [16]. The frictional force at the wall is scaled with the slip length [11]. Not unlike viscosity, changing the slip length will influence the wetting rate, but not the final distribution and configuration of the resin on the fiber surface. The slip length is a parameter that models the interactions at the fiber-resin interface.

Fiber volume fraction and packing

The fiber volume fraction is an important property of composites when considering their strength and stiffness. The fiber volume fraction will be controlled in this study through manipulation of the distance between fibers, measured from axis to axis. Two common packing arrangements for fibers are square and hexagonal packing. The hexagonally packed fibers are modeled with a unit cell in which lines connecting the center of each fiber would form an equilateral triangle. The relationship between the fiber volume fraction, (v_f), fiber radius (r), and distance between fiber axes, (d), will be:

$$v_f = \pi\left(\frac{r}{d}\right)^2 \tag{15}$$

for fibers in a square packing arrangement. For fibers in a triangular packing arrangement, the relationship will be:

$$v_f = \frac{2\sqrt{3}}{3}\pi\left(\frac{r}{d}\right)^2 \tag{16}$$

Experimental setup and procedure

The experimental setup, shown in Figure 5, includes a substrate on which a drop of liquid can be deposited by using a thin wire and a camera to capture time-stamped images of the process.

This experiment was performed by depositing a glycerin drop on a flat glass substrate. Glycerin was used as the test liquid because it has similar properties to the epoxy ultimately being used in the drop-spreading experiment. The surface tension of the glycerin was measured with a dynamic contact analyzer to be 0.07 N/m. A

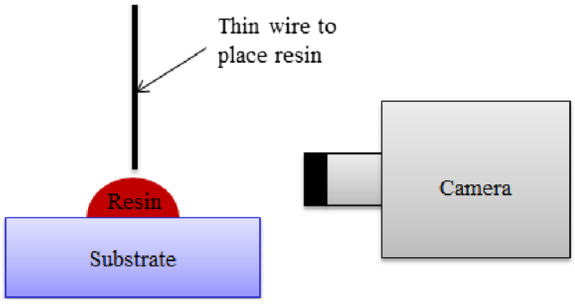

Figure 5 Schematic of the experimental setup to record spreading of a resin drop.

Brookfield DV-E viscometer measured the viscosity of the glycerin to be 0.674 Pa·s. The density of the glycerin, measured using a precision scale and flask, was 1.236 g/cm^3. Sample images of the drop spreading are shown in Figure 6. The static contact angle between the glass and glycerin, measured using image analysis software on the drop in equilibrium, is 28.5°.

Results and discussion

First, experimental and analytical validation of the model used will be provided in the next section before parametric studies are conducted to investigate the dynamics of resin spreading.

Validation of the numerical model

The physics involved in the preceding models is multiphase fluid flow with a high surface to gravitational force ratio. A model of a drop spreading on a flat plate was developed to experimentally verify that the governing equations could predict an acceptable numerical solution to a multiphase wetting dynamics dominated by surface forces.

Comparison between experimental and numerical results

Two experimental trials were conducted of a drop spreading on a flat plate. The first experiment was used to determine the value of β which defines the resin fiber surface characteristics. A β value of zero would correspond to the case where the liquid will not wet the substrate, and an infinite value would describe the scenario where the liquid would reach its final configuration instantaneously. The β value in real systems will fall between the preceding extreme cases and can be determined experimentally by comparing the numerical and experimental solutions using a range of β values. As β is increased or decreased, the wetting rate in the numerical solution will become higher or lower. The β value that describes the liquid-substrate system is found by adjusting the β value until the dimensionless length, defined as the drop length at time t divided by the final length of the drop, matches the experimental results. This experiment used

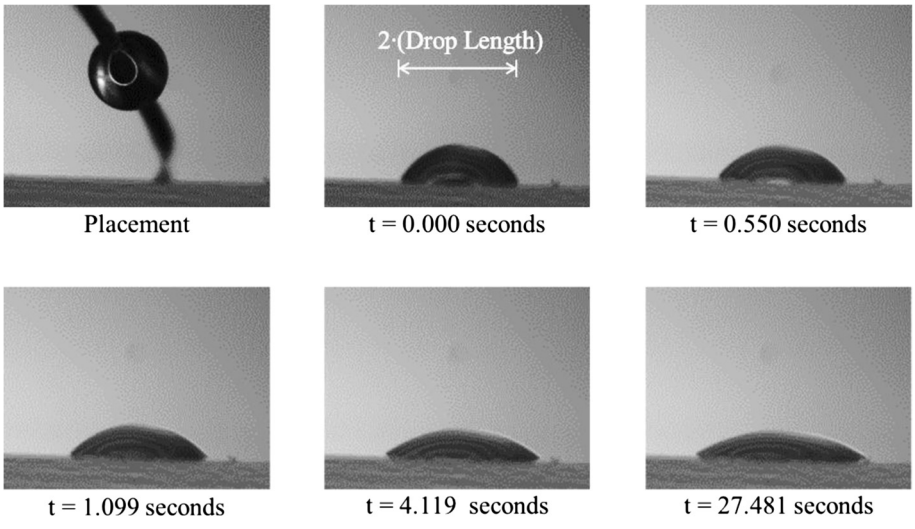

Figure 6 Experimental results depicting spreading of the resin drop as a function of time.

the resin volume of 0.057 mm^3. The β value for slip length from this case was determined to be 0.25 μm. The experimental and COMSOL results for this β value are shown in Figure 7 along with an inset that describes distance β (slip length) below the solid surface and assumes simple shear flow in the region between the wall and the no slip plane.

Having determined the β value, the next experiment was conducted with a drop volume of 0.140 mm^3. The dimensionless length of the COMSOL simulation is compared to the experimental dimensionless length in Figure 7 using the characterized β value. Comparing the results verify the numerical model used to describe the dynamics of resin spreading on a surface for a large surface force to body force ratio.

Mesh-refinement study

A mesh-refinement study was performed to ensure that the numerical results converged as the number of elements in the mesh was increased. Wetting length, as shown in Figure 1, will be used as the characteristic output parameter studied for the axisymmetric model of resin wetting a single fiber. The area of the fiber-resin interface will be used as the characteristic output parameter for the three-dimensional model of resin spreading on a single fiber. Comparing the four solutions for each, depicted in Figure 8, confirms that the numerical output converges and the lowest mesh density used provides an acceptable result.

Comparison of final drop shape with an analytical solution

The equilibrium solution for the axisymmetric model of resin spreading on a fiber was compared to the resin configuration predicted by Carroll [2]. In the numerical solution, resin volume, fiber diameter, and final contact angle are all known. These values were substituted into Equations 3, 4, and 5 and then substituted into Equation 6 to create an equation with one unknown, allowing one to solve for y_0. Once y_0 is known, it can be substituted back into Equations 1 to 4 to develop a parametric equation for x and y. ϕ was varied for values corresponding to $y > r$. The resin-air interface shape at the yz-plane is solved by using this method and is compared to the numerical solution in

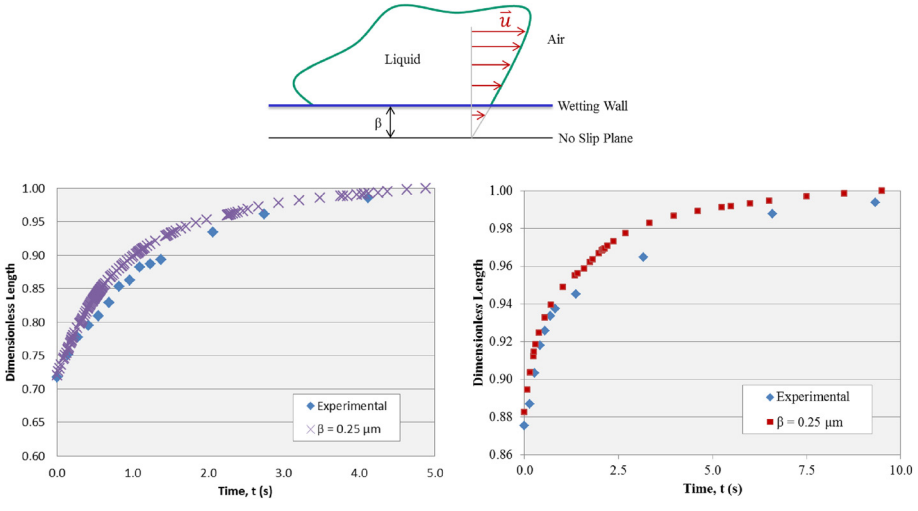

Figure 7 Comparison of numerical model and experimental data for a drop of volume of 0.057 mm^3 (left) and 0.140 mm^3 (right).

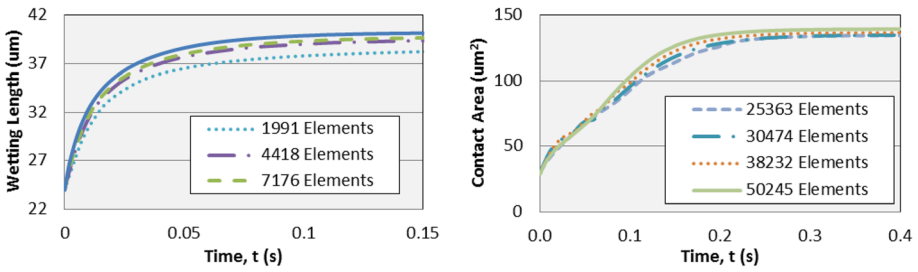

Figure 8 Mesh-refinement study for the axisymmetric (left) and three-dimensional (right) drop spreading on single-fiber models.

Figure 9. The closeness of the two solutions provides further validation of the numerical model.

Parametric study of axisymmetric model

The wetting physics in the axisymmetric model was influenced by the static contact angle, slip length, fiber and resin geometry, and viscosity.

Static contact angle between fiber and resin

The evolution of non-dimensional wetting length over time is shown in Figure 10 for a range of static contact angles. The baseline values are used for all other properties. Here, the non-dimensional wetting length is normalized by the initial wetting length. Fiber-resin interface surface properties with high-contact angles reach their equilibrium position at a lower time because the resin does not travel very far. As the wetting properties are increased, evidenced by a lower contact angle, the amount of the fiber surface covered by the resin increases. The trends found in the contact angle study can be translated to changes in the surface energy of the solid-resin, solid-air, or resin-air through Equation 14.

Resin volume

The volume of the resin impacted both the final wetted length and the rate of wetting as can be seen from Figure 11. The fiber and resin properties are equal to the baseline values. The initial wetting rate was similar for the different resin volumes, but it can be

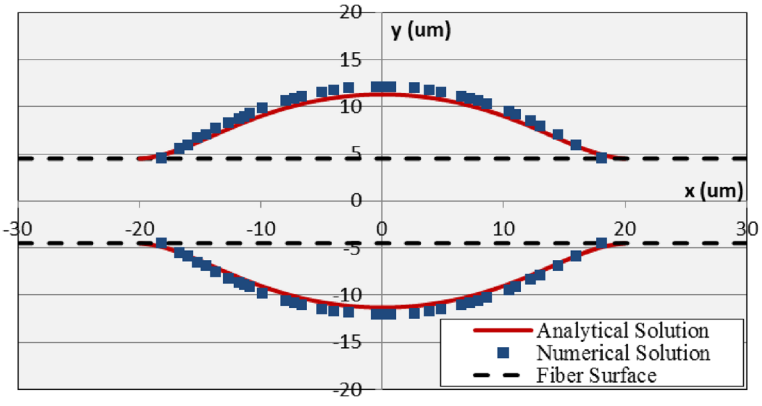

Figure 9 Comparison of the analytical and numerical solutions for the final shape of the resin-air interface.

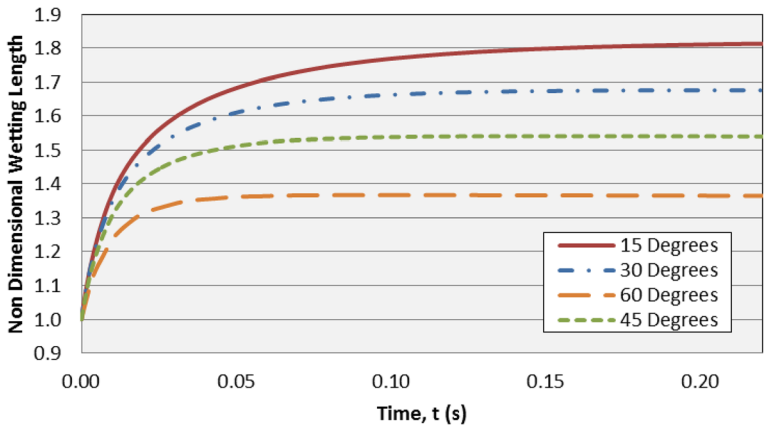

Figure 10 Time-dependent non-dimensional contact length for selected contact angles.

seen that smaller resin drops reached equilibrium faster. This is a result of the resin having to travel a shorter distance and the surface force to resin volume increasing.

Fiber radius

The non-dimensional wetting length, as a function of time for various fiber radii is depicted in Figure 12. The baseline values are used for the fiber and resin properties. All of the initial wetting lengths were slightly different due to the radius of the resin drop changing slightly to keep the resin volume constant for a varying fiber radius. At low times, the resin moves at a similar rate for all trials. With increasing time, the resin reaches equilibrium on the smaller fibers first because it has to travel less and the capillary forces are stronger. The final wetting length increases as the fiber radius was increased due to the resin trying to minimize its surface area.

Slip length

With the exception of the slip length, all properties were equal to their baseline values for this study. The slip length, which characterizes the fiber-resin interface property, did not impact the final wetting length of the resin on the fiber. It did impact the wetting rate as shown in Figure 13. As one would expect, the system reached equilibrium at a faster rate when the slip length was increased due to the increase in slip velocity at

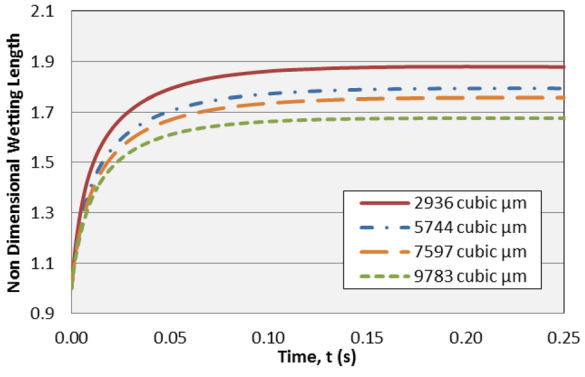

Figure 11 Non-dimensional wetting length versus time for selected volumes (left).

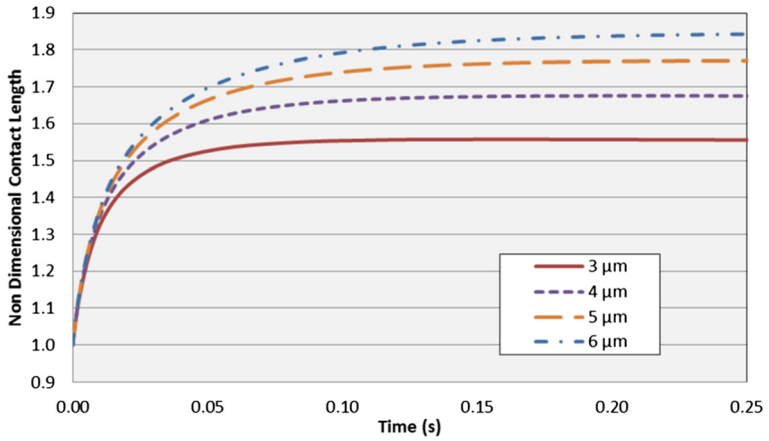

Figure 12 Evolution of contact length over time for selected fiber radii.

the fiber surface. The slip length found in the experimental validation of the physics would fall close to the middle of the values studied.

Three-dimensional single-fiber model

In the three-dimensional model, resin wets the top of the fiber faster than it wets around the circumference of the fiber, depicted in Figure 14. The curvature of the surface slows the rate of wetting on the outside of a concave surface because more resin surface area is created per unit length traveled. The wetted length on the top of the fiber decreases slightly after the resin begins to spread along the bottom of the fiber, the time of which is indicated by the plateau of the circumferential spreading curve.

Square and hexagonal packing fiber unit cells

The spreading of a finite volume of resin within three- (hexagonal packing) and four-fiber unit cells (square packing) with a fiber volume fraction of 30%, static contact angle of 30°, and fiber radius of 4 μm is shown in Figure 15. The interface is described by the level set function, described by the scale bar where a value of one represents purely

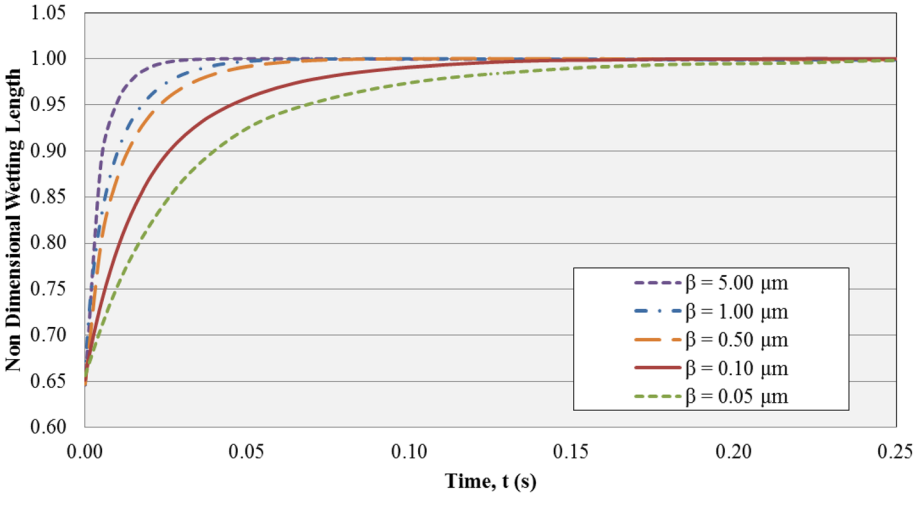

Figure 13 Evolution of non-dimensional wetting length over time for selected slip lengths, *β*.

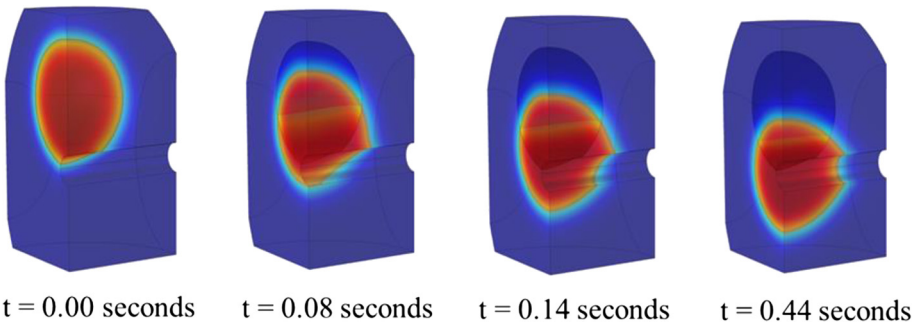

Figure 14 Three-dimensional spreading of a finite volume of resin on a single fiber.

resin. The resin spreads axially and circumferentially along the fiber. The four-fiber unit cell spreads and reaches equilibrium at a much faster rate (0.38 s) than the three-fiber unit cell (1.47 s). This is a result of there being an increased fiber-resin contact area in the four-fiber unit cell.

Fiber volume fraction

For this study, the base parameters were used and the spacing between fibers was varied. The effect of changing fiber volume on the fiber-resin contact area increased as the fiber volume fraction was decreased, as shown in Figure 16. As the volume fraction is changed for the three- and four-fiber unit cells, the spacing between fibers changes at different rates, described in Equations 15 and 16. The change in fiber spacing for the two types of unit cells causes the capillary pressure to change, which can be modeled using the Young-Laplace pressure equation [13]. At larger fiber volume fractions, the capillary pressure increases at a much faster rate, leading to an increased wetted area. At lower fiber volume fractions, the rate of change of capillary pressure is not as high, resulting in a similar increase in wetted area for both types of unit cells. The triangular packing arrangement had a larger fiber-resin contact area per fiber; thus, it would be the preferred packing arrangement if one were to create a network of resin microdrops within a fiber tow with the goal of maximizing fiber-resin contact area.

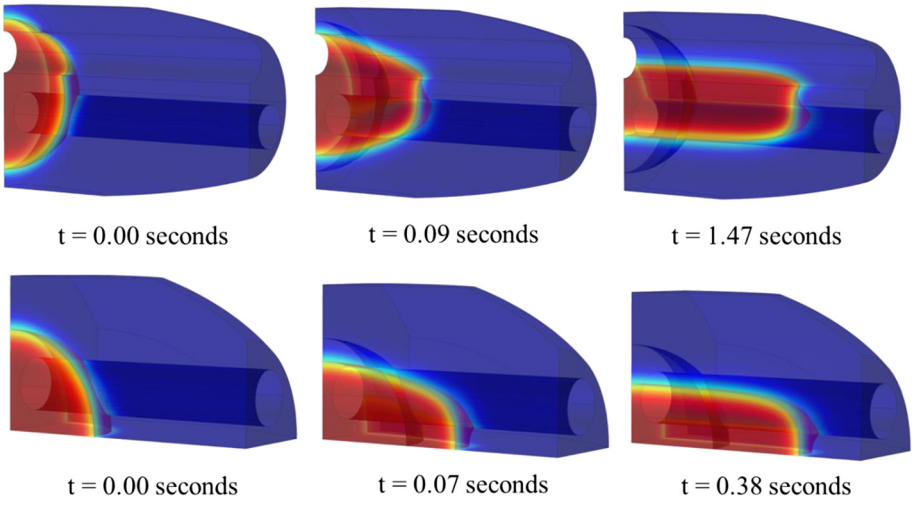

Figure 15 Spreading of resin inside triangular-packed (top) and square-packed (bottom) unit cells at selected time steps.

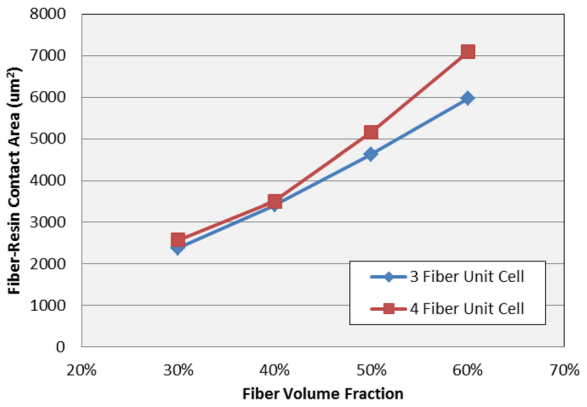

Figure 16 Final fiber-resin contact area as a function of fiber volume fraction.

Static contact angle

The static contact angle had a large effect on the final fiber-resin contact area. The contact area was linear with the cosine of the static contact angle, shown in Figure 17. A linear increase with cos(θ) makes sense because the final results shown are with a fiber volume fraction of 30%. It is clear that for a given fiber volume fraction, the square packing arrangement is preferred for increasing fiber-resin contact area. For this particular combination of resin volume, fiber volume fraction, and fiber size, the ratio of fiber-resin contact area for the triangular and square packing arrangements ranged between 1.07 and 1.11 for the given static contact angles. The static contact angle did not have as significant of an impact on the resin spreading as the packing arrangement did. Resin reached its equilibrium position inside square-packed fibers in about 0.1 to 0.2 s as compared to the 1.1 to 1.5 s with these initial conditions. This indicates that when the same volume of resin wets fibers in a square packing arrangement, the resulting composite will have a higher fiber-resin contact area and faster processing time when compared to a triangular packing arrangement.

Limitations of the model

A limitation on this model is imposed by the assumption of a microscopic length scale. This is because when the diameter of the fiber or the volume of the resin is increased

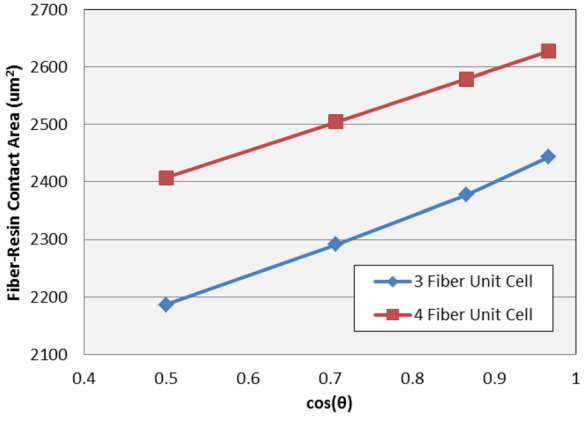

Figure 17 Equilibrium fiber-resin contact area for the three-fiber triangular and four-fiber square packing arrangements.

by a large amount, the inertial and gravitational forces are no longer considered negligible. This would invalidate the axisymmetric assumption in the axisymmetric fiber model. In the four-fiber model, one would no longer be able to use the symmetry plane orthogonal to the direction of gravity. The trends seen in these models may not hold for models with extremely large contact angles because they only examine the case where the liquid will wet the fiber's surface.

Conclusions

Numerical models describing the partial wetting of a finite volume of resin on a single fiber and in triangular- and square-packed unit cells was presented and validated. The static contact angle affected both the rate of axial spreading as well as the final fiber-resin contact area. The volume of resin impacted the final fiber-resin contact area and the wetting rate because larger volumes of resin travel farther. Both the wetting length and final fiber-resin contact area increased with increasing fiber diameter. This claim is only for the case when the resin is in a barrel shape around the fiber as the clamshell shape was not investigated. The slip length had a defined effect on the rate of wetting, but did not impact the final fiber-resin contact area. This indicates that the slip length will not impact the composite properties. Fiber volume fraction had a significant impact on fiber-resin contact area, being more influential at higher fiber volume fractions. The final fiber-resin contact area was larger for square-packed unit cells than triangular-packed unit cells. In unit cells with triangular or square packing arrangements, the static contact angle had a large impact on the final fiber-resin contact area. The effect of static contact angle on wetting rate was small compared to the impact of packing arrangement on wetting rate. These models can be used to predict the impact of manipulating fiber and resin surface properties, interaction, and geometry on the wetting of fibers by a finite volume of resin. By predicting the influence of processing parameters on fiber wetting, one can correlate the resulting microstructure in the unit cell with process and material parameters. The properties of the fibers and matrix can then be used to determine the mechanical properties of a unit cell with the predicted microstructure. The mechanical properties of the unit cells can be used to determine the composite properties.

Competing interests
The authors declare that they have no competing interests.

Authors' contributions
MY did the numerical simulations, analysis, and prepared the article. SGA discussed the numerical results; provided guidance, feedback, and expertise; and revised the article for technical content. All authors contributed significantly to the writing and reviewing. Both authors read and approved the final manuscript.

Acknowledgements
Research was sponsored by the Army Research Laboratory and was accomplished under Cooperative Agreement Number W911NF-12-2-0022. The views and conclusions contained in this document are those of the authors and should not be interpreted as representing the official policies, either expressed or implied, of the Army Research Laboratory or the U.S. Government. The U.S. Government is authorized to reproduce and distribute reprints for Government purposes notwithstanding any copyright notation herein.

Received: 7 October 2014 Accepted: 24 February 2015
Published online: 18 March 2015

References

1. Lavi B, Marmur A (2004) The exponential power law: partial wetting kinetics and dynamic contact angles. Colloids Surf A Physicochem Eng Asp 250(1–3):409–414

2. Carroll BJ (1976) The accurate measurement of contact angle, phase contact areas, drop volume, and Laplace excess pressure in drop-on-fiber systems. J Colloid Interface Sci 57(3):488–495
3. Mchale G, Newton M (2002) Global geometry and the equilibrium shapes of liquid drops on fibers. Colloids Surf A Physicochem Eng Asp 206(1–3):79–86
4. Wu X-F, Dzenis YA (2006) Droplet on a fiber: geometrical shape and contact angle. Acta Mech 185(3–4):215–225
5. Eral HB, De Ruiter J, De Ruiter R, Jung Min O, Semprebon C, Brinkmann M, Mugele F (2011) Drops on functional fibers: from barrels to clamshells and back. Soft Matter 7(11):5138–5143
6. Bedarkar A, Xiang-Fa W, Vaynberg A (2010) Wetting of liquid droplets on two parallel filaments. Appl Surf Sci 256(23):7260–7264
7. Vega M-J, Seveno D, Lemaur G, Adão M-H, De Coninck J (2005) Dynamics of the rise around a fiber: experimental evidence of the existence of several time scales. Langmuir 21(21):9584–9590
8. Slawig, Thomas (2006) PDE-constrained control using COMSOL Multiphysics – control of the Navier–Stokes equations. Tech. no. 2005/26
9. Osher S, Sethian JA (1988) Fronts propagating with curvature-dependent speed: algorithms based on Hamilton-Jacobi formulations. J Comput Phys 79(1):12–49
10. Olsson E, Kreiss G (2005) A conservative level set method for two phase flow. J Comput Phys 210(1):225–246
11. COMSOL Inc., COMSOL Microfluidics User's Guide. 2013
12. Lafaurie B, Nardone C, Scardovelli R, Zaleski S, Zanetti G (1994) Modelling merging and fragmentation in multiphase flows with SURFER. J Comput Phys 113(1):134–147
13. De Gennes P-G, Brochard-Wyart F, Quéré D (2004) Capillarity and Wetting Phenomena: Drops, Bubbles, Pearls, Waves. Springer, New York
14. Bernet N, Bourban P-E, Maanson J-AE (2000) On the characterization of wetting and adhesion in glass fiber-PA12 composites. J Thermoplastic Compos Mater 13(6):434–450
15. Hocking LM (1976) A moving fluid interface on a rough surface. J Fluid Mech 76(04):801–817
16. Andrienko D, Dünweg B, Vinogradova OI (2003) Boundary slip as a result of a prewetting transition. J Chem Phys 119(24):13106–13112